Reference number: PA 2014/260-2.2.1

Linnæus University
School of Computer Science, Physics and Mathematics

Degree Project

Optimizations of inlet box geometry for high pressure axial flow fans

Göran Bäcklund
2011-02-18
Subject: Physics
Level: A
Course code: 4FY84E

Table of contents

1 Introduction

In this chapter the background, goal and outline of the thesis is presented.

1.1 Background

Industrial fans are used in modern boiler plants, to provide oxygen for combustion and to exhaust flue gas via the chimney. Two kinds of fans are used in boiler plants: centrifugal fans and axial flow fans. In the boiler plants axial-flow fans are usually to prefer because they have a higher efficiency, and can transfer a larger amounts of gas than centrifugal fans. To achieve a sufficient increase in pressure a two-stage axial flow fan can be used. If two-stages are not sufficient a centrifugal fan is usually used. Axial flow fans have impellers that force the gas to move parallel in a direction of the fan shaft. An everyday example of an axial flow fan is a ceiling fan or a table fan.

In this thesis a high pressure two-stage axial flow fan is studied. The two-stage axial flow fan is manufactured by Fläkt Woods. The fan has an arrangement of guide vanes in front of the first impeller and between the two impellers. The first guide vane arrangement is curved upstream. For flue gases we get a heat problem for the motor. Even with cold air there is a problem, since the motor affects the airflow and gives large pressure drops. The solution is to use an inlet box and to place the large motor outside the air stream. In the inlet box the gas is re-directed 90 degrees and this gives the fan a non-symmetrical flow profile, upstream the first impeller if there are no upstream guide vanes.

In the fan we have pressure losses between the inlet and the impellers. High pressure loss causes high energy loss and low efficiency. A fan with low efficiency demands much electricity, which causes higher expenses for the boiler plants. We also know that higher pressure loss causes more noise introducing additional cost for acoustic treatment. Earlier simulations on the fan and other experiences have shown that if the velocity profile is more uniform upstream the first impeller, we have beneficial effects on: the efficiency of the whole fan, the pressure, and the aerodynamic and acoustic performance of the fan.

2 Theory

In sections 2.1-2.4 fundamental concepts of fluid flow are presented for readers with no prior knowledge of fluid dynamics. The prerequisites are knowledge in vector calculus. The CFD software used in this thesis is using the time averaged equation presented in 2.5 resulting in a hierarchy of equations with statistical unknown terms modelled by so called closure relations presented in 2.6. In 2.8 and 2.9, theories and studies about flows over aerofoils and guide vanes and how these could be mounted in elbows and bends to lower the pressure losses are presented.

2.1 Rate of change following the fluid

The theory in this section is taken from [3]. A fluid is a gas or a liquid. To describe the rate of change following the fluid we use a velocity vector

$$\vec{u} = \begin{pmatrix} u[x(t), y(t), z(t), t] \\ v[x(t), y(t), z(t), t] \\ w[x(t), y(t), z(t), t] \end{pmatrix},$$

where *u,v* and *w* are the velocity components in the Cartesian *x, y* and *z* directions. By taking the derivative of *u* with respect to *t* and using the chain rule we get the following result:

$$\frac{\partial u}{\partial x}\frac{dx}{dt}+\frac{\partial u}{\partial y}\frac{dy}{dt}+\frac{\partial u}{\partial z}\frac{dz}{dt}+\frac{\partial u}{\partial t} = \frac{\partial u}{\partial t}+u\frac{\partial u}{\partial x}+v\frac{\partial u}{\partial y}+w\frac{\partial u}{\partial z} = \frac{\partial u}{\partial t}+\vec{u}\cdot\nabla u.$$

The derivative of *v* with respect to *t* is

$$\frac{\partial v}{\partial t}+\vec{u}\cdot\nabla v.$$

The derivative of *w* with respect to *t* is

$$\frac{\partial w}{\partial t}+\vec{u}\cdot\nabla w.$$

Multiplying with the density of the fluid ρ we get:

$$\rho\frac{d\vec{u}}{dt} = \rho\left(\frac{\partial\vec{u}}{\partial t}+\vec{u}\cdot\nabla\vec{u}\right).$$

The first term is called the convective acceleration and is the change of velocity over position and the second term is the unsteady acceleration, the change of velocity over position, and is often called the inertia term [3]. A very common notation is

$$\rho\frac{D\vec{u}}{Dt}=\rho\left(\frac{\partial\vec{u}}{\partial t}+\vec{u}\cdot\nabla\vec{u}\right).$$

Two forces act on a fluid: The pressure gradient and body forces, here shown in Euler's equations of motion:

$$\rho \frac{D\vec{u}}{Dt} = -\nabla p + \rho \vec{g} ,$$

where $\vec{g}$ is the gravitational term and p is the pressure. A flow described by Euler's equations is called an ideal flow.

2.2 Viscosity

The theory in this section is taken from [4]. In nature an ideal flow does not exist. Viscous forces also act on a fluid. Viscosity is the resistance of the fluid due to shear stress. An everyday example of fluids with high viscosity is syrup or oil opposite to air that has very low viscosity. In fluid mechanics a force $\vec{F}$ per unit area A is called a stress and there are two important stresses: one who acts perpendicular to the surface called normal stress and the kind which acts tangentially to the surface and is called a shear stress.

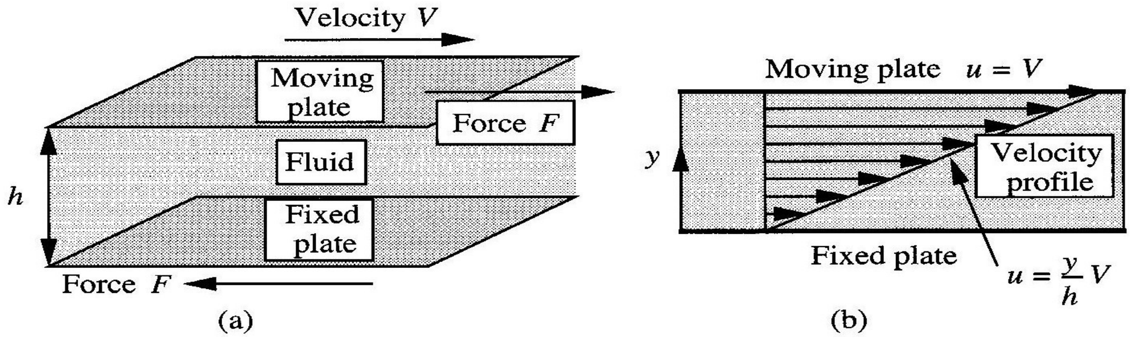

Figure 2.1: a) Fluid in shear between parallel plates b) The ensuing linear velocity profile [4].

Consider a fluid between two solid plates confined in a relative small gap of thickness *h.* One plate is fixed and another plate is moving at a velocity V relative of the fixed plate. The velocity u of the fluid is found to vary linearly from 0 (y=0) to V when using a no slip condition at each plate. The boundary is at rest $\vec{u}=0$ and this condition holds for any viscosity $\nu \neq 0,$ even for very small ones. The velocity is

$$u = \frac{y}{h} V ,$$

then the shear stress that is the tangential applied force divide by the area of each plate become

$$\tau = \frac{F}{A} = \mu \frac{\partial u}{\partial t} = \mu \frac{V}{h} ,$$

where μ is the viscosity and its dimension is kg/(ms). Often the kinematic viscosity is used. Instead it is defined as $\nu = \mu / \rho$ and has the dimension m^2/s.

There are nine stress components acting on any point of the fluid. This is often written as a tensor

$$\boldsymbol{\tau}=\begin{pmatrix}\tau_{xx} & \tau_{xy} & \tau_{xz}\\ \tau_{yx} & \tau_{yy} & \tau_{yz}\\ \tau_{zx} & \tau_{zy} & \tau_{zz}\end{pmatrix}.$$

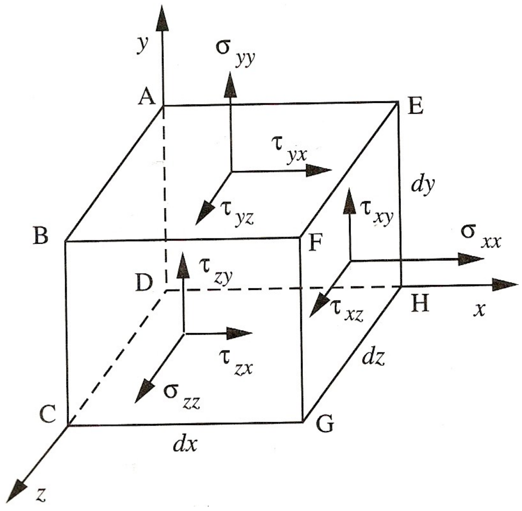

Figure 2.2: the nine normal and shear stress components [4].

The total stress tensor is

$$\boldsymbol{\sigma}=\begin{pmatrix}\sigma_{xx} & \tau_{xy} & \tau_{xz}\\ \tau_{yx} & \sigma_{yy} & \tau_{yz}\\ \tau_{zx} & \tau_{zy} & \sigma_{zz}\end{pmatrix}=\begin{pmatrix}-p & 0 & 0\\ 0 & -p & 0\\ 0 & 0 & -p\end{pmatrix}+\mu\begin{pmatrix}2\frac{\partial u}{\partial x} & \frac{\partial u}{\partial y}+\frac{\partial v}{\partial x} & \frac{\partial u}{\partial z}+\frac{\partial w}{\partial x}\\ \frac{\partial v}{\partial x}+\frac{\partial u}{\partial y} & 2\frac{\partial v}{\partial y} & \frac{\partial v}{\partial z}+\frac{\partial w}{\partial y}\\ \frac{\partial w}{\partial x}+\frac{\partial u}{\partial z} & \frac{\partial w}{\partial y}+\frac{\partial v}{\partial z} & 2\frac{\partial w}{\partial z}\end{pmatrix}.$$

The theory below and section 2.4 is taken from [3]. Using the suffix notation the general equation of motion is defined as

$$\rho\frac{Du_i}{Dt}=\frac{\partial\tau_{ij}}{\partial x_j}+\rho g_i$$

where i and j=1,2,3. The subscript 1,2 and 3 stands for the components in the Cartesian x, y and z directions. For terms with repeated subscript summation over all possible values of that subscript is implied. On substituting the stress tensor into the general equation of motion we get:

$$\rho\frac{Du_i}{Dt}=\frac{-\partial p}{\partial x_i}+\frac{\partial}{\partial x_j}\left(\mu\left(\frac{\partial u_j}{\partial x_i}+\frac{\partial u_i}{\partial x_j}\right)\right)+\rho g_i=\frac{-\partial p}{\partial x_i}+\mu\frac{\partial}{\partial x_i}\left(\frac{\partial u_j}{\partial x_j}\right)+\mu\frac{\partial^2 u_i}{\partial x_j^2}+\rho g_i,$$

where

$$\frac{\partial^2}{\partial x_j^2} = \frac{\partial^2}{\partial x_1^2} + \frac{\partial^2}{\partial x_2^2} + \frac{\partial^2}{\partial x_3^2},$$

and if the fluid is incompressible $\partial u_j / \partial x_j = \nabla \cdot \vec{u} = 0,$ then

$$\rho \frac{D\vec{u}}{Dt} = -\nabla p + \mu \nabla^2 \vec{u} + \rho \vec{g}.$$

The equations above are called the Navier-Stokes equations for an incompressible fluid.

2.3 Reynolds number

Reynolds number is a dimensionless number for a viscous flow in motion and it is defined as

$$Re \equiv \frac{UL}{\nu}$$

where U is the typical flow speed and L is the characteristic length of the flow. The derivative of the velocity component can be written as $O(U/L),$ the convective acceleration or the inertia term as $|\vec{u} \cdot \nabla \vec{u}| = O(U^2/L),$ and the viscous term as $|\nu \cdot \nabla^2 \vec{u}| = O(\nu U/L^2).$ The ratio

$$\frac{|\text{inertia term}|}{|\text{viscous term}|} = O(Re)$$

will give us a good estimation of the relative magnitude of the two most important terms of Navier-Stokes equations.

2.4 Turbulent flow

Flows with very high Reynolds numbers become turbulent. The flows that are not turbulent are called laminar. The region of Reynolds numbers between 2100 and 4000 is called the transition region. Flows with Reynolds numbers over 4000 are likely turbulent.

One good example of laminar and turbulent flow is cigarette smoke. For the first few centimetres the smoke is laminar but when the hot air accelerates upwards it becomes unstable, random and chaotic.

The theory in the last section of this chapter is taken from [5].

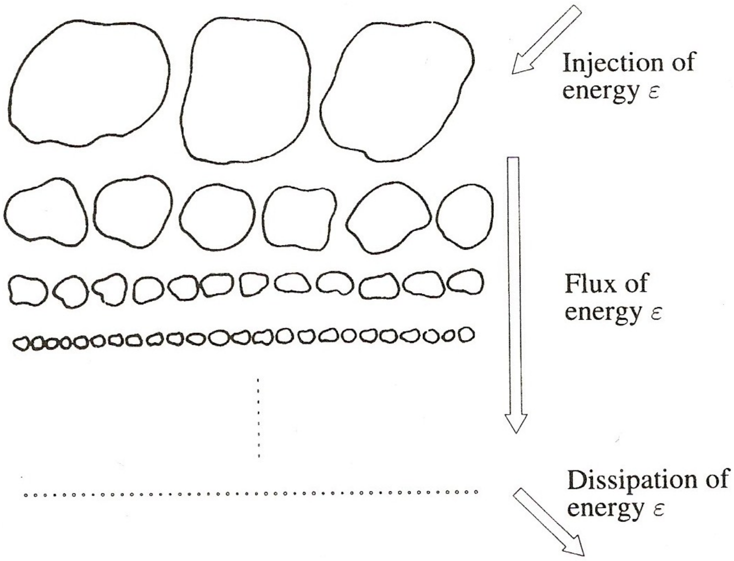

Figure 2.3: The cascade of kinetic energy [5].

ε in figure 2.3 is the kinetic energy dissipated per unit mass and is defined as

$$\varepsilon = \frac{C_D U^3}{2\mathrm{L}} \sim \frac{U^3}{2\mathrm{L}} = \frac{(1/2\,U^2)}{(U/L)} = \frac{\text{Kinematic energy per mass}}{\text{circulation time}},$$

where C_D is known as the dimensionless drag coefficient that will be discussed in section 2.8, and the circulation time is the time it takes for the fluid to move a distance equal to the reference length *L*. Turbulence contains rotational flow structures, so called turbulent eddies with a wide range of length scales. The kinetic energy cascades from the large structures to the small ones, a process that continues creating smaller structures, and the dissipation of energy will take place in the smallest eddies, illustrated in figure 2.3.

2.5 RANS

The theory in this section is taken from [6].

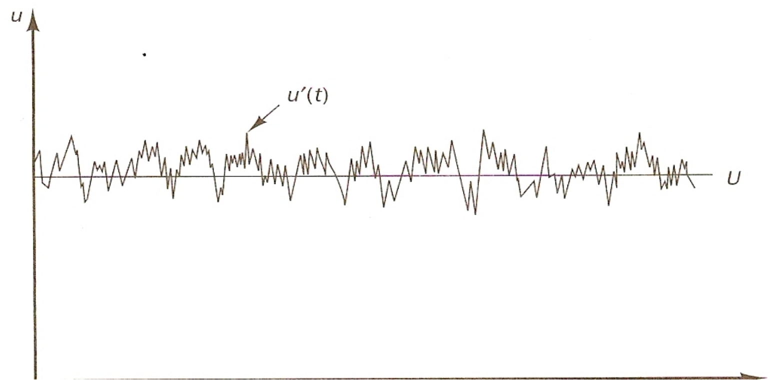

Figure 2.4: A typical point velocity measurement in turbulent flow [6].

A typical point velocity measurement in turbulent flow might look like figure 2.4. With a fluctuating component $u'(t)$ and mean value U superimposed, $u(t)=u'(t)+U$ is called the Reynolds decomposition where the mean U is defined as

$$U=\frac{1}{\Delta t}\int_0^{\Delta t} u(t)\,dt.$$

The Reynolds average Navier-Stokes equations RANS are the time average equations of motion for fluid flow, and can be derived by using the Reynold decomposition: $\vec{u}=\vec{u}'+\vec{U}$, $u=u'+U$, $v=v'+V$, $w=w'+W$ and $p=p'+P$ in the Navier stokes equations of incompressible flow, and with help of the vector identity $\nabla\cdot u\vec{u}=(\nabla u)\cdot\vec{u}+u(\nabla\cdot\vec{u})$. For an incompressible flow, the last term is zero. Navier-Stokes equations can now be written as

$$\rho\frac{\partial u}{\partial t}+\nabla\cdot(u\vec{u})=\frac{-1}{\rho}\frac{\partial p}{\partial x}+\nu\nabla\cdot(\nabla u),$$

$$\rho\frac{\partial v}{\partial t}+\nabla\cdot(v\vec{u})=\frac{-1}{\rho}\frac{\partial p}{\partial x}+\nu\nabla\cdot(\nabla v),$$

$$\rho\frac{\partial w}{\partial t}+\nabla\cdot(w\vec{u})=\frac{-1}{\rho}\frac{\partial p}{\partial x}+\nu\nabla\cdot(\nabla w).$$

The inertia term of the x momentum equation is

$$\nabla\cdot(u\vec{u})=\frac{\partial uu}{\partial x}+\frac{\partial uv}{\partial y}+\frac{\partial uw}{\partial z}\quad=$$

$$\frac{\partial(u'+U)(u'+U)}{\partial x}+\frac{\partial(u'+U)(v'+V)}{\partial y}+\frac{\partial(u'+U)(w'+W)}{\partial z}.$$

This can be rewritten as

$$\nabla\cdot(U\vec{U})+\nabla\cdot(u'\vec{u}') \;=\; \nabla\cdot(U\vec{U})+\frac{\partial u'^2}{\partial x}+\frac{\partial u'v'}{\partial y}+\frac{\partial u'w'}{\partial z}.$$

The result gives us new terms to the equation of motion, and because this is additional turbulent stresses it is customary to put those on the right hand side of the equation

$$\rho\frac{\partial U}{\partial t}+\nabla\cdot(U\vec{U})=\frac{-1}{\rho}\frac{\partial p}{\partial x}+\nu\nabla\cdot(\nabla U)+\frac{1}{\rho}\left(\frac{\partial u'^2}{\partial x}+\frac{\partial u'v'}{\partial y}+\frac{\partial u'w'}{\partial z}\right),$$

$$\rho\frac{\partial V}{\partial t}+\nabla\cdot(V\vec{U})=\frac{-1}{\rho}\frac{\partial p}{\partial y}+\nu\nabla\cdot(\nabla V)+\frac{1}{\rho}\left(\frac{\partial -\rho u'v'}{\partial x}+\frac{\partial -\rho v'^2}{\partial y}+\frac{\partial -\rho v'w'}{\partial z}\right),$$

$$\rho\frac{\partial W}{\partial t}+\nabla\cdot(W\vec{U})=\frac{-1}{\rho}\frac{\partial p}{\partial z}+\nu\nabla\cdot(\nabla W)+\frac{1}{\rho}\left(\frac{\partial -\rho u'w'}{\partial x}+\frac{\partial -\rho v'w'}{\partial y}+\frac{\partial -\rho w'^2}{\partial z}\right).$$

There are six extra stresses, three normal: $\tau_{xx}=-\rho u'^2$, $\tau_{yy}=-\rho v'^2$, $\tau_{zz}=-\rho w'^2$ and three shears stresses: $\tau_{xy}=\tau_{yx}=-\rho u'v'$, $\tau_{xz}=\tau_{zy}=-\rho u'w'$ and $\tau_{yz}=\tau_{zy}=-\rho v'w'$.
These extra turbulent stresses are called Reynold stresses.

2.6 Closure relations

These extra terms are modelled by equations called closure relations. The theory in this section is taken from [6]. First we need some definitions. The instantaneous kinetic energy is the sum of mean kinetic energy and the turbulent kinetic energy $k=K+k'$ where $K=1/2(U^2+V^2+W^2)$ and $k'=1/2(u'^2+v'^2+w'^2)$. The rate of deformation in a mean and fluctuating component is

$$s_{ij}=S_{ij}+s_{ij}'=\frac{1}{2}\left(\frac{\partial U_i}{\partial x_j}+\frac{\partial U_j}{\partial x_i}\right)+\frac{1}{2}\left(\frac{\partial u_i'}{\partial x_j}+\frac{\partial u_j'}{\partial x_i}\right).$$

The governing equation for mean flow kinetic energy can be obtained by multiplying the *x* component in RANS by *U,* the *y* component equation by *V,* and the *z* component equation by *W.* This gives us the equation

$$\frac{\partial(\rho K)}{\partial t}+\nabla\cdot(\rho K\vec{U})=\nabla\cdot(-P\vec{U}+2\mu\vec{U}S_{ij}-\rho\vec{U}u'_iu'_j)-2\mu S_{ij}\cdot S_{ij}+\rho u_i'u_j'\cdot S_{ij}. \quad (2.1)$$

The rate of change of *K* plus the transport of *K* by convection can be seen on the left-hand side of (2.1). The transport of *K* by pressure, viscous stresses and Reynold stresses minus the rate of viscous dissipation of *K*, and minus the rate of destruction of *K* due to turbulence production is found on the right-hand side of (2.1). Similar methods for the turbulent energy give us

$$\frac{\partial(\rho k)}{\partial t}+\nabla\cdot(\rho k\vec{U})=\nabla\cdot(-p'\vec{u}'+2\mu\vec{u}'s'_{ij}-\rho\frac{1}{2}u'_i\cdot u'_iu'_j)-2\mu s'_{ij}\cdot s'_{ij}-\rho u_i'u_j'\cdot S_{ij}.$$

This is similar to (2.1), but here the last term is positive adding turbulent energy and the dissipation per volume is $\rho\varepsilon=2\mu s'_{ij}\cdot s'_{ij}$.

Transport equations for other quantities can be obtained in similar manner. The standard k-epsilon model is using the transport equations for *k* and ε. Using dimension analysis it is possible to write the turbulent eddy viscosity as $\mu_t=\rho C_\mu k^2/\varepsilon$, where C_μ is a modelling constant (see table 2.1). The transport equations for *k* and ε are

$$\frac{\partial(\rho k)}{\partial t}+\nabla\cdot(\rho k\vec{U})=\nabla\cdot(\frac{\mu_t}{\sigma_k}\nabla k)-2\mu_t S_{ij}\cdot S_{ij}-\rho\varepsilon$$

and

$$\frac{\partial(\rho\varepsilon)}{\partial t}+\nabla\cdot(\rho\varepsilon\vec{U})=\nabla\cdot(\frac{\mu_t}{\sigma_\varepsilon}\nabla\varepsilon)+C1_\varepsilon\frac{\varepsilon}{k}2\mu_t S_{ij}\cdot S_{ij}-\rho C2_\varepsilon\frac{\varepsilon^2}{k}.$$

The rate of change of *k* or ε, and the transport of *k* or ε by convection can be seen on the left-hand side of the two transport equations. The transport of *k* or ε by diffusion, plus the rate of production of *k* or ε minus rate of destruction of *k* or ε can be seen on the right-hand side of the equations.

Constant	Value
C_μ	0,09
$C1_\varepsilon$	1.44
$C2_\varepsilon$	1,92
σ_k	1
σ_ε	1,3

Table 2.1

The model constants in the transport equations for *k* and ε shown in table 2.1 is determined from experimental data [6].

The material below and in section 2.7 is taken from [1]. Another option is to model the transport of the dissipation per unit turbulent energy. The turbulent eddy viscosity can be written as $\mu_t = \rho k/\omega$, where $\omega = \varepsilon/k$ is the turbulent frequency. The transport equations for k and ω are

$$\frac{\partial(\rho k)}{\partial t} + \nabla\cdot(\rho k \vec{U}) = \nabla\cdot(\mu_t \frac{1}{2}\nabla k) - 2\mu_t S_{ij}\cdot S_{ij} - \rho\beta_k\omega,$$

and

$$\frac{\partial(\rho\omega)}{\partial t} + \nabla\cdot(\rho\omega\vec{U}) = \nabla\cdot(\mu_t \frac{1}{2}\nabla\omega) - 2\alpha\frac{\omega}{k}\mu_t S_{ij}\cdot S_{ij} - \rho\beta\omega^2,$$

where alpha is a constant $\alpha = 13/25$, and $\beta = 9/125 f_\beta$, $\beta_k = 9/100 f_{(\beta k)}$ are functions. The correction factor f_β is defined as

$$f_\beta = \frac{1 + 70\chi_\omega}{1 + 80\chi_\omega},$$

where χ_ω is defined by

$$\chi_\omega \equiv \left|\frac{\Omega_{ij}\Omega_{jk}S_{ki}}{\left(\frac{9}{125}\omega\right)^3}\right|.$$

Here, the tensor Ω_{ij} is the mean rotation-rate tensor, defined by

$$\Omega_{ij} = \frac{1}{2}\left(\frac{\partial U_i}{\partial x_j} - \frac{\partial U_j}{\partial x_i}\right).$$

The correction factor $f_{(\beta k)} = 1$ if $\chi_k \leqslant 0$ and $f_{(\beta k)} = (1 + 680\chi_k^2)/(1 + 400\chi_k^2)$, if $\chi_k > 0$, where χ_k is defined by

$$\chi_k \equiv \frac{1}{\omega^3}\nabla k\cdot\nabla\omega.$$

5 Analysis

This chapter gives an analysis of how the result in chapter 4 corresponds to the theory in chapter 2.

5.1 Pressure drop

COMSOL calculates the static pressure, and the dynamic pressure is calculated with (2.4). The total pressure difference for the inlet box is $\Delta P_t = P_{(s,inlet)} + P_{(d,inlet)} - P_{(s,outlet)} - P_{(d,outlet)}$. To define the pressure drop in ventilation components a dimensionless *K* value is used. The *K* value for the fan is defined as $K = \Delta P_t / P_{(d,outlet)}$.

Comparing the inlet box geometry with a bend pipe then *K* depends on the hydraulic diameter of the duct. Equation (2.6) and figure 4.25 give us

$$D_H = 2\frac{xy}{(y+x)}.$$

The graphs in figure 4.26-4.28 show *K* as function of D_H. The fit $K = A/D_H$, for figure 4.26 gives us $A = 0.906\,\mathrm{m} \pm 0.030\,\mathrm{m}$. The fit for figure 4.27 gives us $A = 0.944\,\mathrm{m} \pm 0.008\,\mathrm{m}$. The fit for figure 4.28 gives us $A = 0.924\,\mathrm{m} \pm 0.017\,\mathrm{m}$. The three graphs give us a similar proportionality constant at a value of approximately 0.925 m. This gives us the equation

$$K \approx 0.925\,\mathrm{m}\frac{(x+y)}{2xy}. \tag{5.1}$$

According to table 4.13 we get the lowest *K* value for $a_{(n+1)}/a_1 \approx 3$ see (2.7). We have a higher *K* value for $a_{(n+1)}/a_1 < 3$, and $a_{(n+1)}/a_1 > 3$, which corresponds very well with the theory of guide vanes mounted in bends and elbows presented in section 2.9.

The hydraulic diameter of the inlet can be found in table 4.15, and is $D_{(H\,inlet)} = 1.197\,\mathrm{m}$. For the outlet, the cross-section area *A* and the perimeter *p* can be calculated with COMSOL, which give us $A = 0.75\,\mathrm{m}^2$ and $p = 5.38\,\mathrm{m}$. Now, (2.7) gives us $D_{(H\,outlet)} = 0.139\,\mathrm{m}$. *S* can be calculated with the hydraulic mean diameter for the inlet and for the outlet to $S = \sqrt{D^2_{(H\,inlet)} + D^2_{(H\,outlet)}} \approx 1.2\,\mathrm{m}$. The calculated result for *S* in (2.8) gives us an optimal distance of

$$a_1 = \frac{1.2}{(2+1)}\left(0.5 + \frac{(1-1)}{2}\right) = 0.2\,\mathrm{m},$$

and

$$a_{(n+1)} = a_3 = \frac{1.2}{(2+1)}\left(0.5 + \frac{(3-1)}{2}\right) = 0.6\,\mathrm{m},$$

which correspond well with table 4.13 and 4.14, where the lowest *K* value is at $a_1 = 0.20\,\mathrm{m}$ and $a_{(n+1)} = 0.61\,\mathrm{m}$.

5.2 Lift, drag and circulation

In this section we compare the graphs in figure 5.1 taken from [2] with the graphs for guide vanes 1 to 5, which can be found on pp. 28-34, in this thesis.

Recall that the vorticity is proportional to the circulation, and the lift coefficient is proportional to the total lift force, see (2.2), and (2.3). When comparing the graphs we see that the vorticity graphs for guide vane 1 to 5 are similar to the graph of the circulation in figure 5.1.

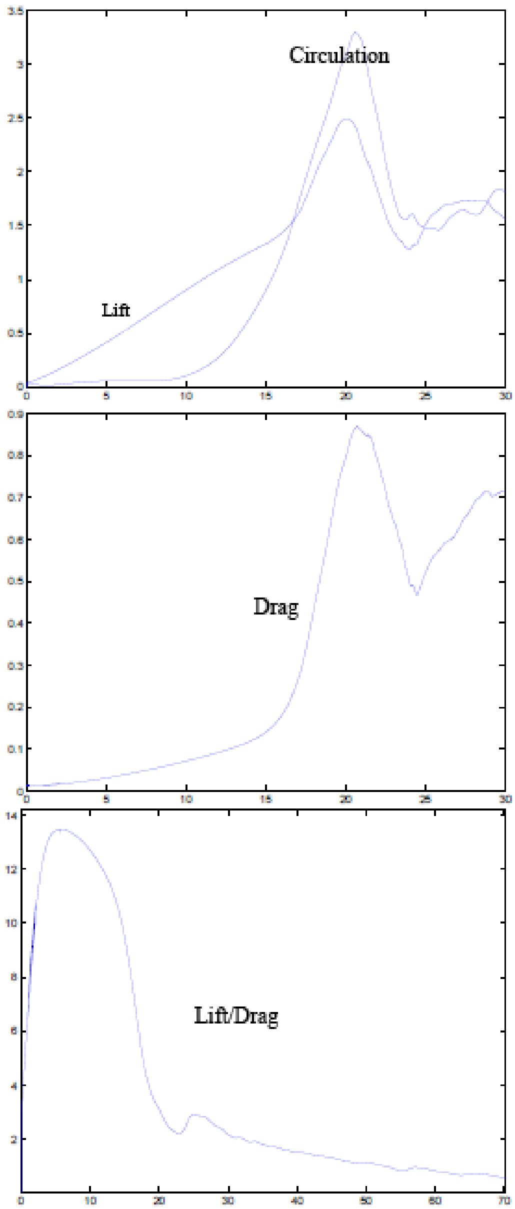

Figure 5.1: The top graph shows the lift coefficient and circulation as functions of angle of attack. The middle graph shows the drag coefficient as functions of angle of attack. The bottom graph shows the C_L/C_D ratio as functions of angle of attack [2].

The middle graph in figure 5.1 is similar to the graph of the lift coefficient in figure 5.1. The same similarity between F_L, and F_D can be found in the graphs for guide vane 1 to 5.

In the graphs for guide vane 1 to 5 we get the top in F_L/F_D for higher value of the radius and the top in the vorticity for lower value of the radius. When we compare the bottom graph and the circulation in the top graph in figure 5.1, we have an opposite situation. This because we have defined a radius instead of an angel of attack. The highest value for the efficiency F_L/F_D is at R=0.120 m for guide vane 1, at R=0.110 m for guide vanes 2-3, and at R=0.115 m for guide vanes 4-5.

Adjusting the curvature of the small guide vanes gave according to the theory higher circulation. We see from our cross-section slices that the velocity distribution is similar for the simulations for the different radius. The data from the simulations also shows that we get a similar K value for all radius.

5.3 Evaluation of the software

It was not possible to import the CAD geometry to COMSOL. CAD geometries are not constructed for finite element analyses. For that reason we had to draw our own geometry. The differences from the real geometry could have an effect on the simulations. When adjusting the curvature of the small guide vanes. We had to redraw the guide vanes with a different radius for each simulation. Mistakes when redrawing the geometry could have an effect on the result. COMSOL's CAD tools are not the right CAD software to use when working with detailed geometries.
Simulations using a different boundary settings for the inlet gave similar result, which shows consistence in the numerical method.

In reference [11] a simulation using COMSOL was carried out to calculate the drag coefficient of a sphere, and the results have showed an excellent agreements with known results, which verify the numerical method.

6.Conclusions

In this chapter, our own conclusions are presented.
The simulations have shown that by adjusting the curvature of the small guide vanes we do not gain much in improved efficiency. We get at most a 5% decrease in pressure drop, and we only get a small improvement of the velocity profile upstream the impellers.

The simulation with large guide vanes in the inlet box gives an improved efficiency if we remove the small guide vanes. The small guide vanes are used to stabilize the construction. For that reason the curved part of the small guide vanes are removed. When using small guide vanes, we do not gain or lose in efficiency by installing large guide vanes in the inlet box. The result is still of interest because this design is easier and have a lower cost to construct.

By increasing the size of the inlet box we can improve the efficiency. We get a 15% decrease in pressure drop, when we increased the size of the inlet box with 20%. By doubling the size of the inlet box we get a 30% decrease in pressure drop. The simulation also shows an improvement in the uniformity of the velocity profile.

The best alternative of the geometrical modifications investigated in this thesis is therefore to increase the size of the inlet box.

References

[1] D.C. Wilcox, *Turbulence Modeling for CFD,* DCW industries Inc., 1998.

[2] J. Hoffman and C. Johnson, The Mathematical Secret of Flight*, Nordisk Matematisk Tidskrift 57:4,* pp. 6-9, 2009.

[3] D.J. Achenson, *Elementry Fluid Dynamics,* Oxford Applied Mathematics and computing series, 1990.

[4] J. Wilkes, *Fluid Mechanics for Chemical Engineers with Microfluidics and CFD,* Prentice Hall, 1999.

[5] U. Frisch, *Turbulence The Legacy of A. N. Kolmogorov,* Cambridge university press, pp. 92-104, 1995.

[6] H.K. Versteeg and W. Malalasekera, *An Introduction to Computational Fluid Dynamics*, Prentice Hall, pp. 63-67, 1995.

[7] Y. Nakayama and R. Boucher, *Introduction To Fluid Mechanics,* Butterworth-Heinemann, 1999.

[8] B. Massey and J. Ward-Smith, *Mechanics of Fluids,* Stanley Thornes Ltd, pp. 339-351, 1998.

[9] I.E. Idelchik, *Handbook of Hydralic Resistance,* Begell House, pp. 199-203, 2001.

[10] A. Durbin, On the $k-\varepsilon$ stagnation point, *International Journal of Heat and Fluid Flow,* vol.17, pp. 89-90, 1986.

[11] R.Sangjin, CFD-based Evaluation of Drag Force on a Sphere Unsteadily
Moving Perpendicularly toward a Solid Surface: a Simple Model of a Biological Spring, *Vorticella Convallaria. 2008 COMSOL User Conference*, 2008.

Linnæus University
School of Computer Science, Physics and Mathematics

SE-351 95 Växjö / SE-391 82 Kalmar
Tel +46-772-28 80 00
dfm@lnu.se
Lnu.se/dfm